Some Observations on Colocated and Closely-Spaced Strong Ground Motion Records of the 1999, Chi-Chi, Taiwan Earthquake

by Guo-Quan Wang, David M. Boore, Heiner Igel, and Xi-Yuan Zhou

Abstract: Model A-800 and A-900A digital accelerographs were colocated at 22 stations that recorded the 1999 Chi-Chi, Taiwan, earthquake. Comparisons of the amplitude, frequency content, and baseline offsets from several of the colocated accelerographs A-800 records differ significantly from the A-900A records. On this basis, and in view of the more thorough pre-deployment testing of the more recent A-900A instruments, we recommend that the records from the A-800 instruments be used with caution, if at all, in analyses of the mainshock and aftershocks. At Hualien seismic station two A-900A instruments were colocated. Although the records are much more similar than those from a colocated A-800 instrument, both records contain unpredictable baseline offsets, as do many of the strong-motion data from this event, and the details of the baseline offsets differ considerably on the two three-component records. There are probably numerous sources of the baseline offsets, such as tilting of the ground and background noise, but for the two colocated A-900A records at the Hualien seismic station, the differences in the baseline shifts suggest that the source is some transient disturbance within the instrument itself-----this is a form of instrument self-noise. The baseline offsets generally manifest themselves in the acceleration time series as pulses or steps, either singly or in combination. We find a 0.01 Hz low-cut filter can almost completely eliminate the effects of the baseline offsets, but then information regarding the residual displacements is lost. The real mechanisms of the baseline offsets are unknown presently. Hence, it is very difficult to recover the residual displacements from the modern digital records, although for records close to large earthquakes, the signal-to-noise ratio should theoretically be adequate to obtain ground motions with periods of hundreds of seconds. This study reinforces our conclusion from previous studies that the sources of baseline offsets occurring in digital strong-motion records are very complex and often unpredictable, and that therefore it is difficult to remove the baseline effect so as to maximize the information content of the record. The baseline offsets only affect very long-period motions, however, and therefore are of no engineering concern.

Introduction

The Chi-Chi, Taiwan earthquake (Mw=7.6; Sep.20, 1999, 17:47:15.9 GMT; located at 23.8603N, 120.7995E) produced the largest set of digital strong-motion data ever recorded from a single earthquake. After this event, scientists from Taiwan and the U.S. made an intensive effort to make the data available as soon as possible for scientists worldwide. About 441 digital three-component free-field strong-motion records of the mainshock were published by the Central Weather Bureau of

Taiwan (CWB) (Lee et al., 1999, 2001a). Among the 441 accelerographs, there are 22 A-800----A-900A pairs that were installed at the same station. Comparisons of these colocated records are helpful in understanding the problem of baseline offsets occurring in near-fault records of this event (e.g., Boore, 2001). As far as we know, a robust procedure for the correction of the baseline offsets that is applicable to all near-fault recordings of this event has not been proposed. In order to develop such a procedure, the sources of the baseline offsets must be understood. As one way of contributing to this understanding, we compare carefully the records from three colocated instruments (HWA, HWA019 and HWA2) installed at the Hualien seismic station. In addition, records from two stations (HWA013 and HWA014) that are very close to the Hualien seismic station are also analyzed. The locations of the sites mentioned in this study are shown in Figure 1.

For the problem of baseline offsets occurred in the Force-Balance Accelerometers (FBA), many researchers had done a series researches (Amini and Trifunac, 1985; Iwan et al., 1985; Novikova et al., 1992; Chiu, 1997; Boore, 1999; Boore, 2001; Wang, 2001; Chiu, 2001; Shakal et al., 2001). In order to obtain quantitative data on the background noise of a typical digital strong-motion recorder, a Kinemetrics PDR-1/FBA-13 instrument was tested by Iwan et al. (1985). For the instruments that they were testing, they attributed the source of the baseline shift to a mechanical or electrical hysteresis within the transducer system that occurred when acceleration exceed about 50 cm/s^2. The consequence was that the baseline could be changing in a complicated way during the interval of strong shaking. In our previous researches (Boore 2001; Wang, 2001; Wang et al. 2001a), we introduced a simple correction scheme that firstly a line is used to fit the latter portion of uncorrected velocity trace (the intersection of the line with the zero axis was named as t_0), then remove the slope of the fitted line from the original acceleration (from t_0 to end). For some very strong near fault ground motion records, the baseline offsets are significant. A reasonable permanent displacement can be obtained after this correction. This study shows that offsets can occur even for relatively weak motions, and the simple correction based on the intersection of a line fit to velocity with the zero axes is not enough to correct for the baseline offsets that produced the displacement trends for the records we have studied. The baseline offsets for the records studied here can produce uncertainties of up to 80 cm in displacement, which is small compared to the residual displacements near the fault (which can be hundreds of cm). There might be a combinations of effects, some related to the level of shaking and some intrinsic to the instrument. The latter is what probably occurred on most of the records that we have studied, and indicate the level of "random" or aleatory uncertainty in the residual displacements. In this paper we will make a detailed study of records from the colocated and closely-located instruments to see if we could differentiate the sources causing the baseline offsets.

Data Sources and Processing

The A-800 accelerograph is a 12-bit digital data recorder and contains three Geotech Model S-110 accelerometers that are mounted orthogonally inside a cast aluminum base. The piezoelectric transducers have a low-cut frequency of 0.02 Hz, and in addition the datalogger includes a 0.1 Hz

low-cut filter. Data are stored in CMOS static RAM using a non-distorting format without data compression (Lee et al., 2001a). The A-900 has all the features of the A-800 while being upgraded with a 16-bit resolution. A very important difference is that it uses Geotech Model S-220 Force Balanced Accelerometers (FBA), which have a flat response to DC, and does not include low-cut filtering. The A-900A accelerograph is an improved version of the A-900, which has the following two additional features: submersible to 2 m, and a real-time digital data stream in USGS Real-Time Digital Telemetry System format. On the A-900 and A-900A, a GPS-1 receiver can be used to synchronize the internal timing (http://www.geoinstr.com/A-900.htm). The data resolution is 0.489 and 0.0598 gal/count for the 12-bit A-800 and the 16-bit A-900/A accelerographs, respectively (Liu et al., 1999). Some physical parameters of A-800 and A-900/A models are listed in Table 1.

All the A-800 and A-900/A accelerographs have three channels, and the trigger algorithm allows a threshold setting for individual channels. In reality, however, a common triggering mechanism is used for the three channels. Once one is triggered, the other two will also be triggered. That is, the three channels are recorded at the same time (W.H.K. Lee, written commun., 2001). Timing is mostly based on the accelerograph's internal clock. However, the time from this clock may not be the same as GMT time. Both the A-800 model and A-900/A models use a trigger algorithm and a buffer, so that the pre-trigger part of the ground motion is captured, which is very important in obtaining the zero level. The accelerograph locations (latitude, longitude, elevation), distances (distance to source, to rupture surface, to the horizontal projection of the rupture surface, and to the surface outcrop of the rupture surface), and instrumental models are listed in Table 2.

A preliminary correction has been applied to all records used in this study by removing the mean determined from a segment of the pre-event portion of the original record from the whole original acceleration record----this guarantees that the velocity will be zero near the beginning of the record. For simplicity of expression, the resulting accelerations are called "uncorrected" accelerations, although a correction has been applied in fact. In turn, velocities and displacements obtained by single and double integration of the uncorrected accelerations are called uncorrected velocities and uncorrected displacements, respectively. In the strictest sense, the records of the three colocated instruments should be identical, because they represent the ground motion at the same site caused by the same earthquake. To make detailed comparisons of the ground accelerations, as well as the velocities and displacements, it is necessary to provide a common time base for all of the records. Some of the Taiwan free-field accelerographs are equipped with a GPS timing device, but that is not the case for the five accelerographs studied in this article. Although the instrument internal time can be obtained, the internal clock is initialized manually, and is no better than about 1 second initially. Hence, it is necessary to correct the start times of the most records. Table 3 lists the corrected GMT time of the record start and P-arrival supplied by Lee et al. (2001a).

Study of Records from Colocated Instruments

An indication that there are systematic differences between the A-800 and A-900A records comes from the ratios of peak accelerations from the 22 colocated A-800 and A-900A instruments. The specific information of the 22 pairs are listed in appendix table. As seen in Figure 2, on average the

peak accelerations for the A-800 instruments are smaller than those from the A-900A instruments. We have made a more detailed study of the records from the three colocated instruments at the Hualien seismic station. This station is classified as a soil site (NEHRP class D, Lee et al., 2001b), with a distance to the epicenter of 83 km. The three instruments HWA (A-800), HWA019(A-900A) and HWA2(A-900A) were mounted on a single concrete seismic pier. The surface size of the seismic pier is 2.0 m by 3.0 m, with a height of about 0.6 m. The two A-900A models were separated by 0.5 m, and the A-800 model was placed next to one of the A-900A models (W.H.K. Lee, written commun., 2001). A Global Position System (GPS) instrument was also installed at the Hualien seismic station. The coseismic displacements estimated from the GPS measurements are -0.8 ± 0.9 cm, 3.7 cm and -21.3 cm for the UP (negative represents down direction), NS (positive represents North direction) and EW (negative represents West direction) components, respectively (Yu et al., 2001).

Figure 3 illustrates the uncorrected accelerations of the three colocated instruments HWA (A-800), HWA019 (A-900A) and HWA2 (A-900A). The acceleration time series of the two A-900A instruments (HWA019, HWA2) coincide very well in both the amplitude and phase during the whole time series. According to our careful observations of superimposed accelerograms, however, there are slight differences between the A-800 and A-900A accelerograms both in their amplitude and phase. The amplitudes of the A-800 records are slightly smaller than those of the A-900A models throughout the time series for all three components. Integrating to velocity and displacement provides a way of comparing the longer period components of motion. The results are shown in Figure 4. At sufficiently long time after the strong shaking, the ground velocities should be essentially zero, and the displacement time series should be constant and equal to the permanent displacement produced during the earthquake. However, what we see as a digital "record" is not the actual time series of the ground accelerations, but the response or output of the accelerograph to the input motions.

As illustrated in the Figure 4, our expectations of what the ground motion should be are not met for the colocated records at Hualien: the velocities from the recordings on the A-800 instrument do not oscillate around zero, and the displacements for all records show no signs of leveling off at the end of the records (at a time well beyond the expected duration of strong shaking) (Wang et al., 2001a). These problems are due to what we call baseline offsets-----small steps or distortions in the reference level of the acceleration (Iwan et al., 1985; Chiu, 1997; Boore, 1999; Boore, 2001). Baseline offsets occur in both the A-800 and A-900A records, but they seem more severe for the A-800 records. These findings are consistent with accumulating experience that the outputs of high-quality digital instruments are often plagued by baseline problems (e.g., Boore, 2001; Boore et al., 2002). The difference in the trends of the displacements for the same component of motion on the three colocated instruments indicates that the baseline offsets are not common to all instruments, as would not be the case for ground rotation (Trifunac and Todorovska, 2001) or ground tilt, either transient or permanent. This suggests that the source of the baseline offsets must be internal to each instrument. The trends in the displacement records from the A-800 instrument imply a significant amount of long-period energy in the record. This energy must have been introduced in the record within or after the analog-to-digital conversion and not from actual motion of the ground,

indicating that the problem is in the datalogger. We can say this with certainty because the A-800 instrument uses a high-pass piezoelectric transducer and also includes a 0.1 Hz high-pass filter before the A/D converter (J. Kerr, oral commun., 2001; W.H.K. Lee, written commun., 2001).

The latter portions of the velocity traces of the UP and NS components of HWA (A-800) have the form of a constant step occurring at somewhere around 45 to 65 sec, with an amplitude of 3 to 5 cm/s (Figure 4a, c). Such a step could be produced by a short-lived (pulse-like) offset in the baseline of acceleration trace; this would give an unrealistic displacement that grows linearly with time at the end of the record (Figure 4b, d). The EW component of the velocity waveform from the A-800 instrument diverges from the velocities from the A-900 instruments over the whole record (Figure 4e). As a result, the displacement waveforms of the A-800 instrument are substantially different from those of the A-900A instruments. The velocities of the two A-900A records show nearly no differences for the UP and NS components (Figure 4a, c), and there are only very slight differences in the amplitudes for times well after the strong shaking has ceased on the EW component (Figure 4e). All and all, the differences in the velocity traces of the two A-900A models are insignificant. The very small differences are enlarged, however, in the displacement traces. The displacement traces from both A-900A instruments are almost identical for the first 60 sec, after which they diverge. At the end of the displacement traces, the differences are up to 20.3 cm (UP), 19.3 cm (NS) and 138.7 cm (EW) for the three components. It seems that baseline offsets occurred at times around 60 sec, resulting in the trends in the displacements.

Estimates of the coseismic displacement calculated from the colocated GPS measurements are also illustrated in Figure 4. We say "estimates" because the values were obtained as the difference in GPS measurements made before and after the earthquake, and the values could contain pre- and post-event motion, as well as coseismic motion. The preseismic and postseismic displacements are insignificant compared with the displacements produced during the earthquake according to the research of Yu et al. (2001), particularly for the sites far from the causative fault. The Hualien GPS station is a continuous site. The coseismic displacements were calculated using the data one day before and one day after the Chi-Chi mainshock (Yu, written commun., 2001). During the time space about two days, the impact of preseismic and postseismic deformation can be essentially neglected. For this reason, we assume that the GPS measurements are a good estimate of the actual coseismic motion, and from now on we will refer to the GPS values as "coseismic" displacements without qualification. The values of the last displacements (D-last) from the twice-integrated accelerograms and the coseismic displacements are compared in Table 5. It can be seen all of the last displacements of the displacement time series are much larger than the corresponding coseismic displacements, particularly for the A-800 records.

For further analysis of the difference in amplitude and frequency contents of the three colocated records, their Fourier spectra and response spectra are studied. Figures 5 and 6 show the Fourier acceleration spectra and the 5%-damped pseudo-acceleration response spectra obtained from the uncorrected accelerations of the three colocated instruments, respectively. To capture the differences due to the drifts in the displacements, the response spectra have been computed for oscillator periods up to 1000 sec(before computing the response spectra, zeros were added to the

end of the acceleration time series so that the total duration exceeded the oscillator period). Both types of spectra from the two A-900A records agree very well for periods less than 100 sec. The spectra for records from the A-800 instrument do not agree as well, however, particularly at long periods (low frequencies).

The above comparisons of the three colocated records in accelerations (Figure 3), velocities and displacements (Figure 4), Fourier spectra (Figure 5), and response spectra (Figure 6) strongly suggest to us that there are some serious problems with the response and calibration of A-800 type accelerographs. The above analysis seems to confirm the advice of the publishers of the Chi-Chi data------"users are advised not to use the A-800 accelerograph records" (Lee et al., 2001a). This caution was not based on the detailed comparisons such as we have shown here, but rather on the fact that the A-800 instrument was an older model, and had not been rigorously tested by the team that installed the strong-motion network in Taiwan. In view of our detailed comparisons, we suggest that records from A-800 instruments not be used in analyses of either the mainshock or the aftershock data. We have only limited discussion of the A-800 records in the rest of this paper.

Study of Records from Closely-Spaced Instruments

This section compares the records of three closely-spaced instruments HWA013(A-900), HWA014(A-900), and HWA019(A-900A) (and its colocated instrument HWA2(A-900A)). The specific locations of the three sites are shown in the Figure 1b. The durations, which is a bracketed duration with a threshold of 50cm/s^2 of the uncorrected accelerations, of ground motions recorded by different records are listed in Table 4. All of the three stations locate on the soil site (classified as NEHRP class D, Lee et al., 2001b). The greatest horizontal distance between any two sites is less than 1.5 km (1.45 km between HWA019 and HWA013, 1.0 km between HWA013 and HWA014, 0.72 km between HWA014 and HWA019). The elevations of the three sites are 16 m (Hualien station), 9 m (HWA013) and 3 m (HWA014), respectively. We expect the site differences to be small.

The instruments are relatively far from the fault, with a distance to the fault rupture surface of about 54 km and a distance to the epicenter about 82 km. The source-to-site distance and source-to-site azimuth for the three sites are listed in the Table 2. Site-to-site differences in the ground motion due to source and path effects should be minor. If a set of stations is spaced at distances small compared to the wavelengths of a frequency band of interest and if the variation of material properties is not appreciable within the immediate vicinity of the array, there should be little distortion of a long-period disturbance as it crosses the array. For example, for periods greater than about 3 sec, with wavelengths of approximately 10 km or longer, they should be little distortion of signal amplitudes across an array of the dimension of 1 to 2 km or less. In the limit of infinitesimal station spacing, this correlation is exact. Any differences in long-period amplitudes must then be attributed to instrumental or processing errors (Hanks, 1975). For digital records, the processing errors are very small (Iwan et al., 1985; Chiu, 1997). Because of the intrinsic smoothing process of integration and the relative increase in the long period content of the time series, the ground displacements should be more coherent than the ground velocities, which in turn should be more

coherent than the ground acceleration. Because of this and the small inter-station spacing, we assume that the actual ground displacements at all of the three closely spaced stations were nearly identical.

Figure 7 shows the uncorrected displacements of the four A-900/A instruments. In this comparison, the records of the four instruments are aligned according to the absolute GMT time. No attempt was made to use time shifts to align the traces. Calculations of the relative time delays for P or S arrivals between the three stations found that the delays were smaller than 0.5 sec. The displacement traces are similar to one another within the first 60 sec for all three components, particularly for the displacements of the two colocated instruments. Beyond 60 sec, however, the displacement traces begin to diverge. The form of the trend in displacement gives some information about the cause of the baseline shift, but it does not provide enough information to correct unambiguously for the baseline offset. It seems that the trends in some displacement traces are linear, which means a short-duration pulse occurred in the baseline of the acceleration. Of course a curved line could be looked straight for a small segment of axes. For cautious, we inspect the displacement traces in an enlarged figure. For easy to see the linearity of the trend, we use a line to fit the later portion (from 75 sec to end) of the displacement. Figure 8 shows the latter segment (75—130 sec) of the two colocated displacement traces but with a large scale. The least-squared lines are also illustrated in the figure. It can be seen the trends in the displacement traces of HWA019-UP, HWA2-UP, HWA019-NS, HWA2-NS, HWA019-EW are really linear, but the trend in the displacement of HWA2-EW are nolinear**.** From the Figure 7, it is easy to say the trend in the displacements of HWA013-UP, HWA013-NS, HWA014-NS, and HWA014-EW are parabolic, suggesting a step change in the acceleration baseline. But for the HWA014-UP (Figure 7a), it seems that there is no trend occurred in the displacement trace. It can be seen that the degree and characters (linear or parabolic) of the trends occurred in the displacements are probably different for the same component of the different instrument, as well as for the different components of the same instrument. The above observations suggest us that the trends are strongly dependent on the accelerometers of the instruments.

The most interesting observation from the Figure 7 is that the differences of the trends in the displacements of EW component is larger for the colocated instruments (HWA019 and HWA2) than for the closely-spaced, but not colocated instruments. Furthermore, the drifts for the EW components of HWA019 and HWA013 are very similar, and the displacements compare well during the whole time series (Figure 7c), suggesting a common origin for the baseline offsets. HWA013 is an A-900 instrument, whereas HWA019 is an A-900A instrument, presumably not manufactured during the same production run, and thus making it less likely that the cause of the baseline shift is instrumental. It might be that in general the sources of the baseline shifts are both instrumental and noninstrumental. If so, then for all but the EW component of HWA013 and HWA019, the noninstrumental shifts are masked by instrument- and component-specific baseline offsets. The apparent lack of instrument-specific baseline offsets make the EW components of HWA013 and HWA019 particularly interesting, with the hope that corrections can be made for the baseline offsets in order to recover the true ground displacement; this is explored in the next section.

Figures 9 and 10 show the Fourier acceleration spectra and the 5%-damped pseudo-acceleration response spectra of the three closely spaced records HWA013, HWA014 and HWA019. As the response spectra and Fourier spectra of the two colocated records (HWA019 and HWA2) are similar for periods out to 100 sec (and have been compared in previous figures) the spectra of HWA2 are not shown in Figures 9 and 10. Overall, the spectra of all the records are similar. The differences for shorter periods might be due to differences in local site response. The spectra are similar for periods between about 3 sec and 100 sec, as we would expect given the similarity in the sites, the small distances between stations, and the large source-to-site distance. The differences for periods greater than about 100 sec reflect the dissimilar drifts in the displacements at long times.

Correcting for Baseline Offsets

The different character of the drifts in displacements at long times, even for the same component of motion, suggests that the sources of the baseline offset are a form of instrument "noise", and therefore it will be difficult, if not impossible, to correct for the offsets so as to obtain the residual displacements that the instruments should be capable of providing. As noted before, however, the EW component of the displacements from the records at HWA013 and HWA019 are very similar, suggesting a source of the baseline offset external to the instruments. We explore here whether corrections can be made so as to recover the EW component of ground displacement. Our conclusion is that uncertainties in some of the essential correction parameters are such as to make it not possible to recover the displacements in the absence of other information. We follow that work with a discussion of filtering the records to remove the long-period components of motion. The displacements from all of the A-900/A instruments are very similar if energy at frequencies below about 0.015 Hz is removed (in most cases a cutoff frequency of 0.01 Hz is adequate).

The similarity in the displacement trends for the EW recordings from the non-colocated instruments HWA013 and HWA019 is shown in Figure 8, along with a least-squares line fit to the HWA019 displacements from 75 sec to the end of the record. Although the higher-frequency motions have not died down to the point where the form of the trend is unambiguous, the HWA019 displacements seem to oscillate about the straight line, giving support to the conclusion that the trend is a straight line, which can be produced by a short duration pulse in acceleration, rather than a parabola, as is produced by a step in acceleration. With this interpretation, we have corrected the record of HWA019-EW by assuming a pulse in acceleration of 1 sec duration, with amplitude such that the area of the pulse equals the slope of the line fit to the displacement (other pulse durations give similar results as long as the area of the pulses are constant). The time at which the pulse occurs is a free parameter, and we show in Figure 11a the results of placing the pulse at a series of times. As can be seen from that figure, the residual displacement is highly sensitive to the location of the pulse. Placing the pulse at 65 sec gives good agreement with the GPS estimate of the coseismic displacement, which is why 65 sec was chosen. In addition, the divergences in the displacements for the other closely-located stations and for the other components of motion strongly suggest a pulse around 60 sec. In many cases, however, closely-spaced or colocated stations and GPS station are not available, and therefore there would be no control on the time at which the pulse occurs. Because the higher frequency shaking has not ceased, we were concerned

that the fitted line could be sensitive to the segment of the displacement used in the least-squares fit. We tested this by varying the start time of the fit from 75 sec to 110 s; the slopes of the fitted lines are not sensitive to the line segment used in the fit, and as a result, neither are the corrected displacements (Figure 11b).

Another method for correcting of baseline offsets is a generalization by Boore (1999, 2001) of one proposed by Iwan et al. (1985), which assumes that shifts in the baseline occur between some interval of strong shaking and can be accounted for by a pulse followed by a step in acceleration (see Boore, 2001, Figure 4 for an example). The duration and location of the pulse is specified by the first and last occurrences of acceleration exceeding a threshold acceleration. Iwan et al. (1985) "option 1" used a threshold of 50 cm/s^2, based on the particular instrument that they studied. Because there is no reason to assume that this threshold applies to the A-900 instruments, we have used different values from 20 cm/s^2 to 90 cm/s^2. The results are shown in Figure 12, which shows that the correction is not too sensitive to the choice of the exceedance threshold. The corrections, however, are sensitive to the time interval used in determining the straight line fit, as seen by comparing the left and right figures, which used 90 sec and 100 sec start times for the fit, respectively. The sensitivity to the start time is due to several factors: 1) the method is based on fitting a straight line to velocity rather than to displacement, as in the previous correction method, and the slope of the velocity is very small for the EW component of HWA019, and 2) the higher frequency shaking has not ceased, making the slope of the line fitted to velocity sensitive to the continued shaking superimposed on the overall trend (the least-squares fitted lines are shown in the middle row of Figure 12).

Both correction schemes considered here can produce corrected displacements that look similar, with a relatively constant displacement after the interval of strong shaking. There is no inconsistency in this result, because the slope of the velocity is small, and therefore the difference between a parabola or a straight line in the displacement trace is not as pronounced as it would be if the slope were larger. Because of the small slope, the correction based on assuming a linear velocity, rather than a step in velocity, requires a pulse in acceleration just as does the first correction method discussed above. This is shown in Figure 13, which shows the baseline offsets corresponding to some of the corrections considered here. Note the different scales for the ordinate in two parts of the figure. In addition, note the small amplitudes of the pulses (and the pulse height could be reduced to a fraction of the indicated height by increasing the pulse duration by the inverse of this same fraction). These would be difficult to detect by looking at the recorded acceleration time series--- the pulses will not stand out as "spikes".

As we have shown, the problems of baseline offsets generally manifest themselves at long-periods. Hence, low-cut (high-pass) filtering is often used to minimize the effects of baseline offsets. Such a procedure, however, clearly precludes extracting permanent displacement from the records. In this study, a series of low-cut filters are used to eliminate the baseline offsets occurring in the records of the four A-900/A instruments. Figure 14 shows the filtered displacement waveforms of the four instruments, using low-cut frequencies of 0.005, 0.010, and 0.015 Hz. A fourth-order Butterworth causal filter was used. The agreement between the ground displacements at the three stations has

been considerably improved after the low-cut filtering. With the increase of corner frequency of the filters, the overall waveforms (which are controlled by long periods) of the different components become more and more consistent. For the two colocated records, a 0.005 Hz low-cut filter can eliminate most of the differences in the overall character of displacement waveforms (Figure 14, top row); a 0.01 Hz low-cut filter produces close agreement for all but the NS component from HWA013 (Figure 14, middle row); and a 0.015 Hz low-cut filter brings all of the traces into good overall agreement (Figure 14, bottom row). Of course, low-cut filtering does not change the relative differences at high frequencies. These differences are most pronounced for the NS component. The EW component and, in particular, the UP component waveforms are in excellent agreement for all frequencies. Response spectra for the various low-cut filters are shown in Figure 15. Clearly, the response spectra for periods of engineering concern are not affected at all by the presence of the long-period noise.

After 0.01 Hz or higher low-cut filtering, instrument “noise” was eliminated, but of course the energy content below 0.01 Hz was also cut off. We cannot say, however, that the A-900/A instrument is incapable of making useful recordings of motions at frequencies less than about 0.01 Hz; what is important is the relative amplitude of the signal and the "noise". Consider a baseline offset given by a step in acceleration---its Fourier spectrum goes as 1/f, and therefore in displacement the spectrum goes as $1/f^3$. So the effect of the “noise” introduced by the baseline offset exists at all frequencies, but clearly it is most important at low frequencies. Whether or not the “noise” is important for any particular filter cut-off will depend on the amplitude of the signal compared to the noise. A record close to the fault will have much more long-period motion than one far away. Therefore we expect that the frequency at which the noise overwhelms the signal will be lower for stations close to the fault than at distant stations.

Discussion and Conclusions

Modern digital instruments have the capability to recover permanent or residual displacements for large earthquakes, but baseline offsets make it difficult in many cases to do so. It has been recognized from the time that records from the Chi-Chi earthquake were first available that baseline drifts are common in most records of the Chi-Chi earthquake (e.g., Boore, 1999; Boore, 2001, Wang, 2001). What has not been clear is whether the baseline offsets are due to something within the instruments or are the response to actual ground motion, either elastic, such as rotations, or inelastic, such as slumping. Boore (2001) argued that similar trends in the displacements from two colocated instruments TCU129(A-900A) and WNT(A-800) (at a station closer to the fault than those studied here) was evidence for permanent ground tilt.

Based on the observations reported herein, the characteristics of baseline offsets are different from instrument to instrument, even different from the various components of a single instrument. The observations in this study and our previous research illustrate the difficulties of understanding the true source of the baseline offset occurring in many digital recordings. We find for the records used in this study that the baseline offset was most probably produced by some intrinsic mechanism within the instrument. We do not know the exact mechanism, although for the instruments studied

in this article, it seems that the change occurs at about 60 sec after the start of the recording. Because of the random nature of the baseline offsets, we cannot think of a universal correction scheme that can be applied to eliminate the baseline offsets. We recommend low-cut filtering to reduce the effects of baseline offsets, but with the resulting loss of information about the residual displacements. As it seems that most often the source of the baseline offsets is within the instruments, we hope that the manufacturers will try to correct the problem so that analysis of future recordings can take full advantage of the resolution and bandwidth of the instruments.

Acknowledgments

We wish to thank W.H.K. Lee for encouragement to do this study and for supplying information about the Hualien seismic station, and thank Shui-Beih Yu for supplying the coseismic displacement information of the Hualien station. The acceleration data were provided by the Central Weather Bureau of Taiwan (Lee et al., 2001a). Discussions with Francis Wu and Chris Stephens were useful, as were the reviews of xxx and yyy. This research was partially funded the Natural Science Foundation of China under the project No.59895410. The first author wishes to acknowledge the German Academic Exchange Service (DAAD) for funding through the International Quality Network: Georisks (http://www.iqn-georisk.de).

References

Amini, A. and M. D. Trifunac (1985). Analysis of a force balance accelerometer, *Soil Dyn. Earthquake. Eng.* **4**, 82-90.

Boore, D. M. (1999). Effect of baseline corrections on response spectra for two recordings of the 1999 Chi-Chi, Taiwan, earthquake, U.S. Geological Survey, Open-File Report, 99-545.

Boore, D. M. (2001). Effect of baseline correction on displacement and response spectra for several recordings of the 1999 Chi-Chi, Taiwan, earthquake, *Bull. Seism. Soc. Am.* **91**, 1199-1211.

Boore, D. M., Christopher D. Stephens, William B. Joyner (2002). Comments on baseline correction of digital strong-motion data: Examples from the 1999 Hector Mine, California, earthquake. *Bull. Seism. Soc. Am.* **92**, in press.

Chiu, H. C. (1997). Stable baseline correction of digital strong-motion data, *Bull. Seiem. Soc. Am.* **87**, 932-944.

Chiu, H.C. (2001). Recovery of coseismic ground motions with permanent displacement from the strong-motion data of the 1999 Chi-Chi, Taiwan Earthquake (abst.). *Seism. Res. Lett.* **72,** 235-236.

Hanks, T. C. (1975). Strong ground motion of the San Fernando, California, earthquake: ground displacements, *Bull. Seism. Soc. Am.* **65**, 193-235.

Iwan, W. D., M.A. Moser, and C.-Y. Peng (1985). Some observations on strong-motion earthquake measurement using a digital accelerograph, *Bull. Seism. Soc. Am.* **75**, 1225-1246.

Lee, W. H. K., T. C. Shin, K. W. Kuo, and K. C. Chen (1999). CWB Free-Field Strong-Motion Data from the 921 Chi-Chi Earthquake: Volume 1. Digital Acceleration Files on CD-ROM, Pre-Publication Version, Seismology Center, Central Weather Bureau, Taipei, Taiwan, December 6, 1999.

Lee, W. H. K., T. C. Shin, K. W. Kuo, K. C. Chen, and C. F. Wu (2001a) CWB Free-Field Strong-Motion Data from the 921 Chi-Chi Earthquake: Processed Acceleration Files on CD-ROM, Strong-Motion Data Series CD-001, Seismological Observation Center, Central Weather Bureau, Taipei, Taiwan, March 31, 2001.

Lee, C. T., C. T. Cheng, C. W. Liao, and Y. B. Tsai (2001b). Site classification of Taiwan free-field strong-motion stations. *Bull. Seism. Soc. Am.* **91***,* 1283-1297.

Liu K.-S., T.-C. Shin, and Y.-B. Tsai (1999). A free-field strong motion network in Taiwan: TSMIP, Terrestrial, *Atmospheric and Oceanic Sciences* **10**, 377-396.

Novikova E. I., M. D. Trifunac, and M. EERI (1992). Digital instrument response correction for the Force-Balance Accelerometer, *Earthquake Spectra* **8**, 429-442.

Shakal, A.F., and C.D. Petersen (2001). Acceleration offsets in some FBA's during earthquake shaking (abst.), Seism. Res. Lett. 72, 233

Wang, G.-Q. (2001). The characteristics of near-fault ground motion caused by the 1999, Chi-Chi, Taiwan earthquake, PhD thesis, Institute of Geology, China Seismological Bureau, 2001(in Chinese).

Wang, G.-Q, X.Y. Zhou, Z.J. Ma, and P. Z. Zhang (2001a). Data files from "A preliminary study on the randomness of response spectra of the 1999 Chi-Chi, Taiwan, Earthquake", *Bull. Seism. Soc. Am.* **91**, 1388-1389.

Wang, G.-Q, X.Y. Zhou, P. Z. Zhang, and H. Igel (2001b). Characteristics of amplitude and duration for near fault strong ground motion from the 1999 Chi-Chi, Taiwan, Earthquake, *Soil Dyn. Earthquake. Eng.* **22**, 73-96.

Yu, S.-B., L.-C. Kuo, Y.-J. Hsu, H.-H. Su, and C.-C. Liu (2001). Preseismic deformation and coseismic displacements associated with the 1999 Chi-Chi, Taiwan Earthquake. *Bull. Seism. Soc.*

Am. **91**, 995-1012.

Institute of Geophysics
University of Munich
Munich, 80333
Germany
wang@geophysik.uni-muenchen.de
igel@geophysik.uni-muenchen.de
(G.-Q.W., H. I.)

U.S. Geological Survey, MS 977
345 Middlefield Road
Menlo Park, California 94025
boore@usgs.gov
(D.M.B.)

School of Architectural and Civil Engineering
Beijing Polytechnic University
Beijing, 100022
P. R. China
zhouxy@solaris.bjpu.edu.cn
(X.-Y. Z.)

FIGURES

Figure 1. Map showing the locations of accelerographs mentioned in this article. The star in the left figure indicates the epicenter of the Chi-Chi main shock, and the line represents the causative fault----Chelungpu fault. The triangles represent the 441 accelerographs whose records were released by the CWB (Lee *et al.*, 1999, 2001a). The solid triangles in the left figure represent the 22 colocated A-800---A-900A pairs, whose locations and recorded peak ground accelerations are listed in the appendix table. The right figure is the enlargement around the Hualien seismic station. Two A-900A (HWA019 and HWA2) and one A-800 (HWA) accelerographs were installed at the Hualien seismic station, and one GPS instrument was also installed at this station. The coseismic displacements obtained from the GPS measurements are -0.8 ± 0.9 cm, 3.7 cm and -21.3 cm for UP, NS and EW component, respectively. The horizontal distance between the Hualien station and the HWA013 station is 1.45 km, between the Hualien station and the HWA014 station is 0.72 km, and between the HWA013 station and HWA014 station is 1.0 km.

Figure 2. Ratio of peak ground accelerations (PGAs) on A-800 and A-900A instruments, plotted against the A-800 peak accelerations.

Figure 3. Comparisons of the three-component acceleration time series obtained from the three colocated instruments HWA(A-800), HWA019(A-900A) and HWA2(A-900A) for which the mean determined from a segment of the pre-event portion of the original record was removed from the whole record. The accelerograms are aligned according to the absolute GMT time of ground motion. The abscissa shows time relative to the GMT time Sep. 20, 1999, 17:47:16.00 (h:m:s).

Figure 4. Comparison of uncorrected velocities and displacements obtained from accelerations recorded by the three colocated instruments HWA(A-800), HWA019(A-900A) and HWA2(A-900A). The uncorrected velocities and displacements were obtained by single and double integration of accelerations for which the pre-event mean was removed from the whole trace. The GPS estimates of coseismic displacements are -0.8+-0.9 cm, 3.7 cm and -21.3 cm for the UP, NS and EW components, respectively, as obtained from a GPS instrument colocated with the accelerometers (Yu et al., 2001). The abscissa shows time relative to the GMT time Sep. 20, 1999, 17:47:16.00.

Figure 5. Fourier acceleration frequency spectra calculated from the uncorrected accelerations recorded by the three colocated instruments HWA(A-800), HWA019(A-900A) and HWA2(A-900A).

Figure 6. 5% damped pseudo-acceleration response spectra calculated from the uncorrected accelerations recorded by the three colocated instruments HWA(A-800), HWA019(A-900A) and HWA2(A-900A). Before computing the response spectra, zeros were added to the end of the acceleration time series so that the total duration exceeded the oscillator period.

Figure 7. Comparison of uncorrected displacements obtained from four closely-spaced instruments

HWA013(A-900), HWA014(A-900), HWA019(A-900A) and HWA2(A-900A) (HWA2 and HWA019 are colocated). The displacements are obtained from doubly-integrated uncorrected accelerations for which the mean of the pre-event portion has been removed from the whole acceleration trace. The abscissa shows time relative to the GMT time Sep. 20, 1999, 17:47:15.00.

Figure 8. A small portion (75----130 sec) of the displacement time series of the two collocated instruments. The lines are the least-squares fitted resulted from 75 sec to the end.

Figure 9. Fourier acceleration spectra calculated from the uncorrected accelerations recorded by the three closely-spaced (but not colocated) instruments HWA013(A-900), HWA014(A-900) and HWA019(A-900A). The Fourier frequency spectra of HWA2 are consistent with those of HWA019 in the whole frequency range as shown in the Figure 5, so the Fourier spectra of HWA2 are not shown in this figure.

Figure 10. 5% damped acceleration response spectra calculated from the uncorrected accelerations recorded by the three closely-spaced (but not colocated) instruments HWA013(A-900), HWA014(A-900) and HWA019(A-900A). The response spectra of HWA2 are almost equal to those of HWA019 for periods less than 100 sec and are not shown here (see Figure 6 for a comparison over the whole period range). Before computing the response spectra, zeros were added to the end of the acceleration time series so that the total duration exceeded the oscillator period.

Figure 11. Displacement for HWA019-EW, corrected by assuming a 1 sec pulse in the acceleration baseline (the area under the pulse equals the step in velocity corresponding to the slope of a line fit to displacement). (left column) Placing the pulse at various times; (right column) Using various values of the beginning time used in the least-squares fitting of the straight line to the end of the displacement (the line was fit to the displacement from the time shown to the end of the record).

Figure 12. Displacement for HWA019-EW, assuming an Iwan et al. correction scheme (a pulse followed by a step in the acceleration baseline). Using different exceedance levels from 20 to 90 cm/s^2, (left column) the beginning time used in the least-squares fitting of the straight line is 90 sec(t2b=90 sec); (right column) the beginning time used in the least-squares fitting of the straight line is 100 sec (t2b=100 sec).

Figure 13. The baseline corrections (removed baseline offsets) for several of the corrections used to produce the displacements in Figures 11 and 12.

Figure 14. The filtered three-component displacements obtained by integration of the accelerations recorded by the closely-spaced instruments HWA013, HWA014, HWA019 and HWA2 (the latter two are colocated). The start time of the time axes is GMT 17:47:15.00. A fourth-order Butterworth causal low-cut filter was applied to the uncorrected accelerations. (upper row): 0.005 Hz low-cut filter; (middle row): 0.01 Hz low-cut filter; (lower row): 0.015 Hz low-cut filter.

Figure 15. 5% damped pseduo-acceleration response spectra calculated from the uncorrected and a

series low-cut filtered (fcut=0.001Hz, 0.003Hz, 0.01Hz, 0.03Hz, and 0.1Hz) accelerations recorded by the EW component of HWA019(A-900A).

Table 1

Characteristics of A-800 and A-900/A Type Accelerographs (Liu *et al*., 1999)

Model	Resolution	Full scale	Digital Counts	Dynamic Range	Response	Sampling rate (sps)	Memory
A-800	12-bit	1g	2048 count/g	72dB	dc to 50Hz	200	1MB
A-900/A	16-bit	2g	32768 count/g	92dB	dc to 90Hz	200	8MB

Table2

Station Locations, Site Class and Instrument Model

Station	Site Condition (NEHRP)	Lat. (deg N)	Long. (deg E)	Elevation (m)	Epdist. (km)	Source -to-site distance (km)	Source-site azimuth (φ, deg)	DJB* (km)	Drup** (km)	D-fault*** (km)	Instrument Model
HWA	D	23.977	121.605	16	83	83.73	78.721	53.65	54.47	91.75	A-800
HWA2	D	23.977	121.605	16	83	83.73	78.721	53.65	54.47	91.75	A-900A
HWA019	D	23.977	121.605	16	83	83.73	78.721	53.65	54.47	91.75	A-900A
HWA013	D	23.978	121.591	9	81.6	82.34	78.506	52.24	53.08	90.30	A-900
HWA014	D	23.973	121.599	3	82.4	83.13	78.751	53.19	54.02	91.15	A-900

* Epdist: Distance (km) from Chi-Chi epicenter (23.8603 deg N, 120.7995 deg E).

* DJB: The closest horizontal distance from the station to the projection of the rupture surface onto Earth's surface.

* *Drup: The shortest distance between the station and the fault rupture surface.

*** D-fault: The shortest horizontal distance from the station to the surface outcrop of the rupture surface.

Table 3

Record Start Time and P-arrival Time (Lee, W.H.K *et al*., 2001)

Station	Observed record start Time* (h:m:s)	Observed P-arrival time* (h:m:s)	Theoretical P-travel time (sec)	P-travel residue ** (sec)	Corrected P-arrival time (GMT, h:m:s)	Corrected record start time (GMT, h:m:s)	Pre-event portion (sec)	Length of record (sec)
HWA	17:47:29.000	17:47:31.424	15.711	0.043	17:47:31.381	17:47:28.956	2.425	103
HWA2	17:47:17:000	17:47:31.890	15.711	0.509	17:47:31.381	17:47:16.481	14.900	133
HWA019	17:47:15.000	17:47:30.239	15.711	-1.143	17:47:31.381	17:47:16.143	15.239	133
HWA013	17:47:12.000	17:47:28.055	15.489	-3.104	17:47:31.159	17:47:15.104	16.655	134
HWA014	17:47:12.000	17:47:25.535	15.609	-5.744	17:47:31.279	17:47:17.744	13.535	131

*The observed record star time and P-arrival time are based on the instrument internal clock.

**P-travel residue = Observed P-travel time - Theoretical P-travel time.

Table 4

Peak Ground Acceleration (PGA), T_1, T_p and T_2, and Duration of the Studied Records

	PGA (cm/s^2)			T_1 (sec)*			T_p (sec)*			T_2 (sec)*			Duration** (sec)		
	UP	NS	EW	UP	NS	EW	UP	NS	EW	UP	NS	EW	UP	NS	EW
HWA	42.590	-107.672	119.135	---	22.36	25.31	29.38	27.93	29.34	---	32.35	38.12	0.0	9.99	12.81
HWA2	47.729	-132.190	129.080	---	35.22	37.22	42.04	40.59	42.05	---	46.40	51.84	0.0	11.18	14.63
HWA019	46.792	-133.568	126.456	---	35.83	39.78	42.35	40.90	42.36	---	47.02	51.62	0.0	11.19	11.84
HWA013	61.197	-114.156	139.727	42.67	40.15	40.59	42.69	41.64	42.48	42.07	45.96	52.58	0.03	5.81	11.99
HWA014	-39.296	-90.113	101.545	---	37.87	38.35	38.75	42.66	39.91	---	45.99	48.39	0.0	8.12	10.04

*T_1, T_p, and T_2 represent the time that acceleration firstly exceed 50 cm/s^2, get the peak value (PGA), and lastly exceed 50 cm/s^2, respectively. The times are counted from the beginning of the record.

**Duration is a bracketed duration with a threshold of 50 cm/s^2. Duration=T_2-T_1.

Table 5

Comparison of the D-last and Coseismic Displacement*

Instrument	UP		NS		EW	
	D-last* (cm)	Cos-Dis.* (cm)	D-last (cm)	Cos-Dis. (cm)	D-last (cm)	Cos-Dis. (cm)
HWA(A-800)	-346.0	-0.8 ± 0.9	-92.9	3.7	38.2	-21.3
HWA019(A-900A)	-36.4	-0.8 ± 0.9	37.0	3.7	-56.3	-21.3
HWA2(A-900A)	-16.1	-0.8 ± 0.9	17.7	3.7	82.4	-21.3

*The last displacements (D-last) were obtained from the uncorrected displacement time series, and the coseismic displacements (Cos-Dis.) were calculated from the colocated GPS measurements.

ppendix Table

Peak Ground Accelerations Recorded by the 22 A-800----A-900A Pairs in the Chi-Chi Earthquake.

Station	Site Class	Lat. (deg N)	Long. (deg E)	Elev. (km)	Epdist*. (km)	DJB** (km)	Drup***. (km)	PGA -UP (cm/s^2)	PGA -NS (cm/s^2)	PGA -EW (cm/s^2)	Instrum Model
WNT	D	23.8783	120.6843	0.11	11.9	1.94	2.21	-310.60	-602.00	-920.70	A-800
TCU129	D	23.8783	120.6843	0.11	11.9	1.94	2.21	-335.00	-610.60	-982.90	A-900A
TCU	D	24.1475	120.676	0.084	34.2	4.35	4.47	-118.20	-186.60	-201.00	A-800
TCU082	D	24.1475	120.676	0.084	34.2	4.35	4.47	-129.30	192.40	-221.00	A-900A
NSY	C	24.4162	120.7607	0.311	61.7	8.75	9.08	-84.20	-150.30	118.70	A-800
TCU128	C	24.4162	120.7607	0.311	61.7	8.75	9.08	-90.38	-162.90	141.10	A-900A
WGK	D	23.6862	120.5622	0.075	30.9	13.28	13.31	175.60	446.00	337.80	A-800
CHY101	D	23.6862	120.5622	0.075	30.9	13.28	13.31	162.10	390.10	-332.70	A-900A
ALS	C	23.5103	120.8052	2.413	38.8	11.2	14.37	85.65	-145.50	212.90	A-800
CHY074	C	23.5103	120.8052	2.413	38.8	11.2	14.37	101.30	158.50	234.60	A-900A
WTP	B	23.2455	120.6138	0.56	70.7	41.86	41.89	30.00	43.55	44.50	A-800
CHY102	B	23.2455	120.6138	0.56	70.7	41.86	41.89	-23.15	48.45	40.49	A-900A
ESL	D	23.8137	121.4328	0.178	64.7	39.73	44.71	56.45	72.25	-66.55	A-800
HWA020	D	23.8137	121.4328	0.178	64.7	39.73	44.71	52.46	66.63	-56.58	A-900A
WSF	E	23.638	120.2217	0.006	63.8	47.7	47.71	32.06	66.99	-64.60	A-800
CHY076	E	23.638	120.2217	0.006	63.8	47.7	47.71	31.40	-70.94	-68.61	A-900A
NSK	B	24.6755	121.3583	0.682	106.6	46.95	48.02	39.72	-53.59	-67.95	A-800
TCU085	B	24.6755	121.3583	0.682	106.6	46.95	48.02	41.39	-52.34	-62.09	A-900A
STY	B	23.1625	120.7573	0.64	77.4	49.92	50.29	-19.62	39.24	-36.37	A-800
KAU050	B	23.1625	120.7573	0.64	77.4	49.92	50.29	22.97	37.14	-41.69	A-900A
HSN	D	24.8022	120.9695	0.034	105.7	52.56	53.16	-26.32	-79.91	54.07	A-800
TCU081	D	24.8022	120.9695	0.034	105.7	52.56	53.16	-36.13	93.13	76.68	A-900A
HWA	D	23.977	121.605	0.016	83	53.65	54.47	42.59	-107.62	119.14	A-800
HWA019	D	23.977	121.605	0.016	83	53.65	54.47	46.79	-133.57	126.46	A-900A
HWA2	D	23.977	121.605	0.016	83	53.65	54.47	47.73	-132.19	129.08	A-900A
SGS	B	23.0817	120.5827	0.278	89	60.28	60.29	-19.14	-37.80	-28.23	A-800
KAU047	B	23.0817	120.5827	0.278	89	60.28	60.29	20.28	-41.93	-32.60	A-900A
ENA	B	24.428	121.7407	0.113	114.5	65.61	66.3	53.59	64.60	63.64	A-800
ILA050	B	24.428	121.7407	0.113	114.5	65.61	66.3	53.35	62.81	-63.58	A-900A
CHK	D	23.0992	121.3653	0.034	102.2	65.18	68.29	-11.96	45.46	-65.56	A-800
TTN014	D	23.0992	121.3653	0.034	102.2	65.18	68.29	-25.18	43.60	-49.11	A-900A
NCU	D	24.97	121.1867	0.134	129	72.41	73.03	-34.45	98.57	-79.43	A-800
TCU083	D	24.97	121.1867	0.134	129	72.41	73.03	-33.08	114.70	-89.24	A-900A
TAI1	D	23.0402	120.2283	0.008	108	79.31	79.31	-20.10	-44.02	87.57	A-800
CHY078	D	23.0402	120.2283	0.008	108	79.31	79.31	-20.94	-43.78	86.85	A-900A
TTN	D	22.754	121.1465	0.009	127.6	94.51	96.67	14.36	-29.19	29.19	A-800
TTN015	D	22.754	121.1465	0.009	127.6	94.51	96.67	-14.12	-30.63	25.36	A-900A
SGL	D	22.7252	120.4908	0.03	129.6	100.83	100.83	8.61	-30.15	-28.23	A-800
KAU048	D	22.7252	120.4908	0.03	129.6	100.83	100.83	-11.78	28.65	38.28	A-900A
PNG	B	23.5672	119.5552	0.011	131	115.79	115.8	-14.36	32.54	-29.19	A-800
CHY075	B	23.5672	119.5552	0.011	131	115.79	115.8	15.19	37.03	-37.03	A-900A
TAW	B	22.3575	120.8957	0.008	166.7	138.21	138.98	-3.35	-5.26	5.26	A-800
TTN016	B	22.3575	120.8957	0.008	166.7	138.21	138.98	-6.04	-9.75	-7.24	A-900A
HEN	D	22.0055	120.738	0.022	205.5	177.98	178.16	9.09	-24.88	-22.01	A-800
KAU046	D	22.0055	120.738	0.022	205.5	177.98	178.16	7.84	-22.49	22.25	A-900A

* Epdist: Distance (km) from the Chi-Chi epicenter (23.8603 deg N, 120.7995 deg E).

**DJB: The closest horizontal distance from the station to the projection of the rupture surface onto Earth's sur face.

***Drup: The shortest distance between the station and the fault rupture surface.

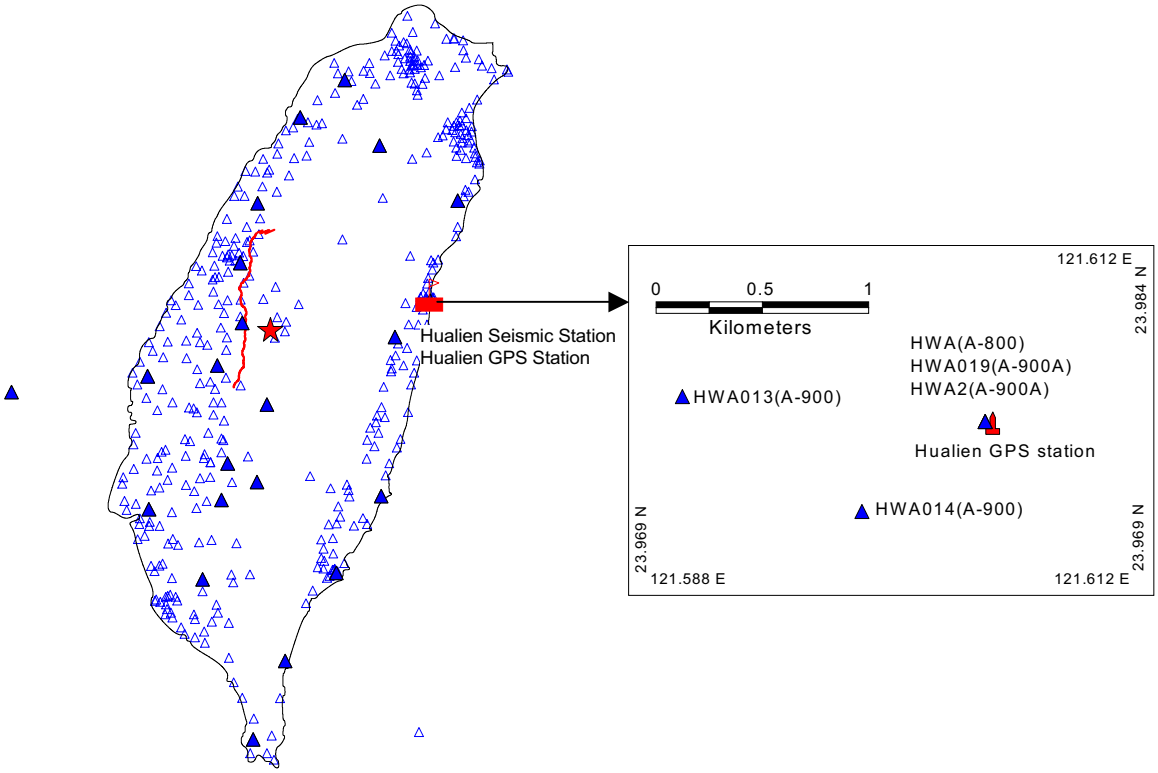

(a) (b)

Figure 1. Map showing the locations of accelerographs mentioned in this article. The star in the left figure indicates the epicenter of the Chi-Chi main shock, and the line represents the causative fault----Chelungpu fault. The triangles represent the 441 accelerographs whose records were released by the CWB (Lee et al., 1999, 2001). The solid triangles in the left figure represent the 22 colocated A-800---A-900A pairs, whose locations and recorded peak ground accelerations are listed in the Appendix Table. The right figure is the enlargement around the Hualien seismic station. Two A-900A (HWA019 and HWA2) and one A-800 (HWA) accelerographs were installed at the Hualien seismic station, and one GPS instrument was also installed at this station. The coseismic displacements obtained from the GPS measurements are -0.8 ± 0.9 cm, 3.7 cm and -21.3 cm for UP, NS and EW component, respectively. The horizontal distance between the Hualien station and the HWA013 station is 1.45 km, between the Hualien station and the HWA014 station is 0.72 km, and between the HWA013 station and HWA014 station is 1.0 km.

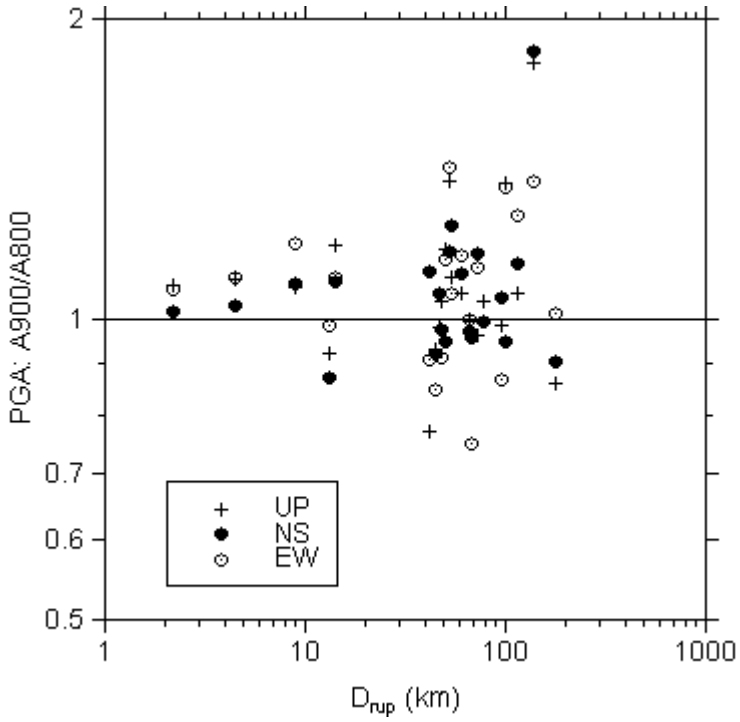

Figure 2. Ratios of peak ground accelerations (PGA---A-900A/A-800) recorded by the 22 colocated A-900A-----A-800 accelerographs. The ordinate represents the PGA ratio of A-900A to its colocated A-800 instrument; the abscissa represents the shortest distance from the station to the causative fault surface. The different marks in the figure represent the three components of ground motion.

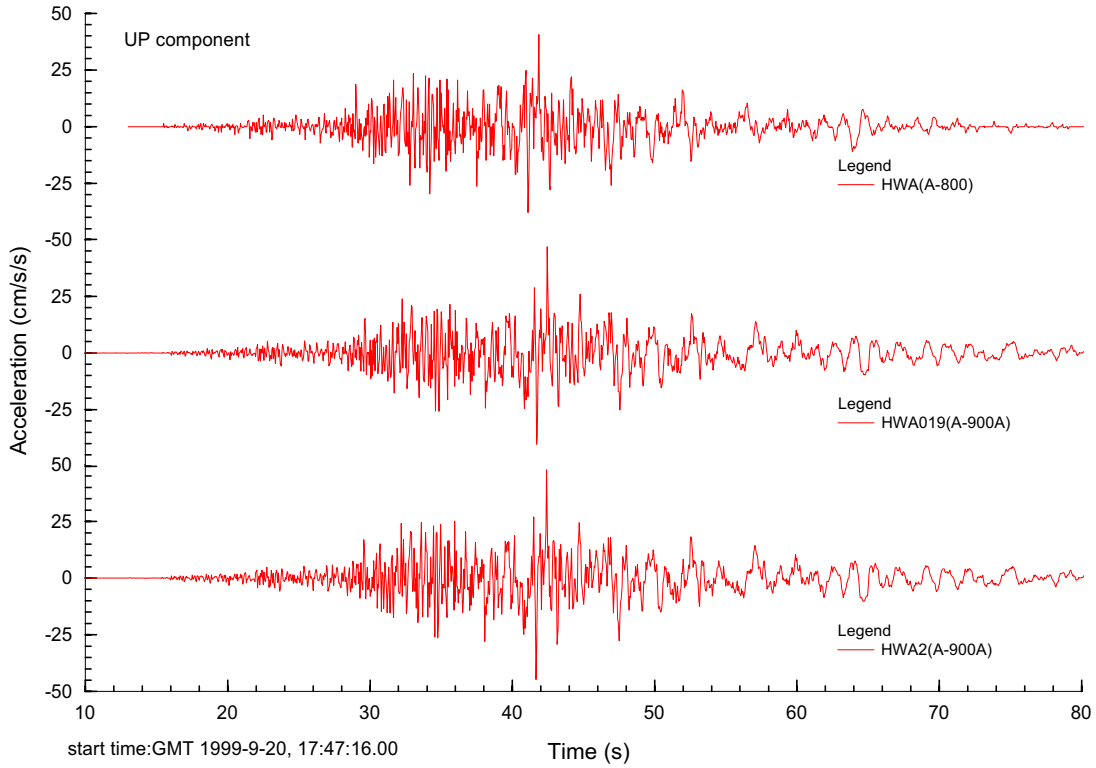
UP component
Acceleration (cm/s/s)
Time (s)
start time:GMT 1999-9-20, 17:47:16.00
Legend
HWA(A-800)
Legend
HWA019(A-900A)
Legend
HWA2(A-900A)

(a)

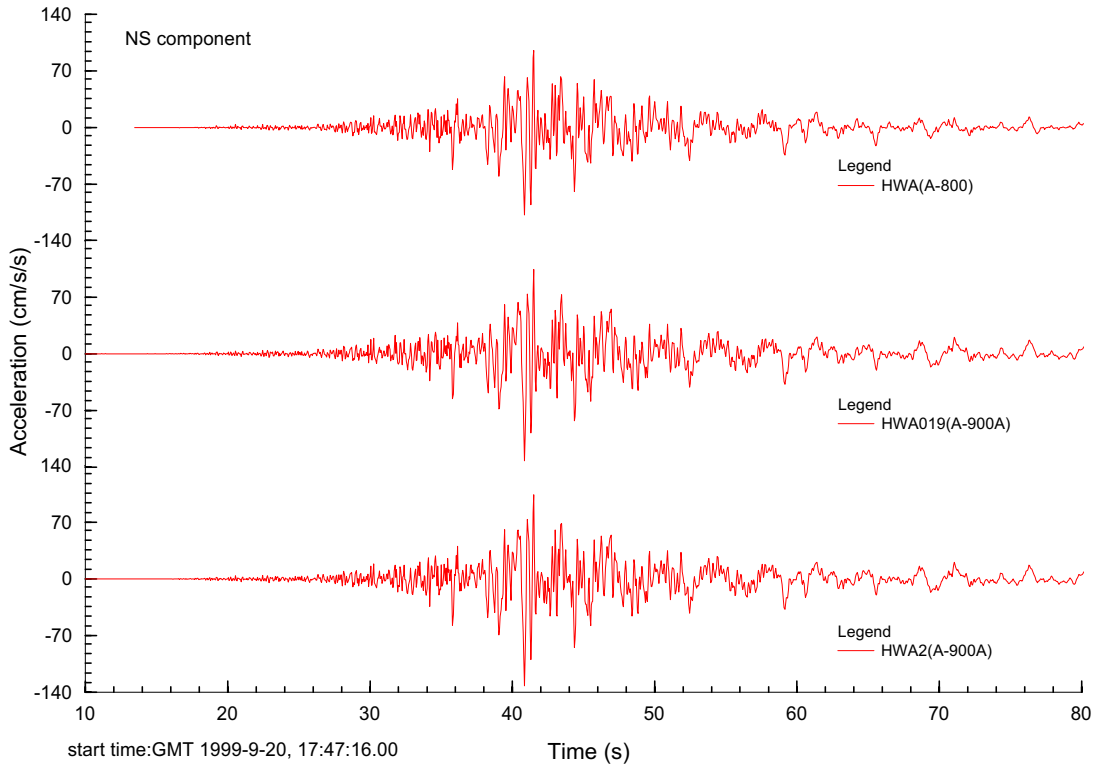
NS component
Acceleration (cm/s/s)
Time (s)
start time:GMT 1999-9-20, 17:47:16.00
Legend
HWA(A-800)
Legend
HWA019(A-900A)
Legend
HWA2(A-900A)

(b)

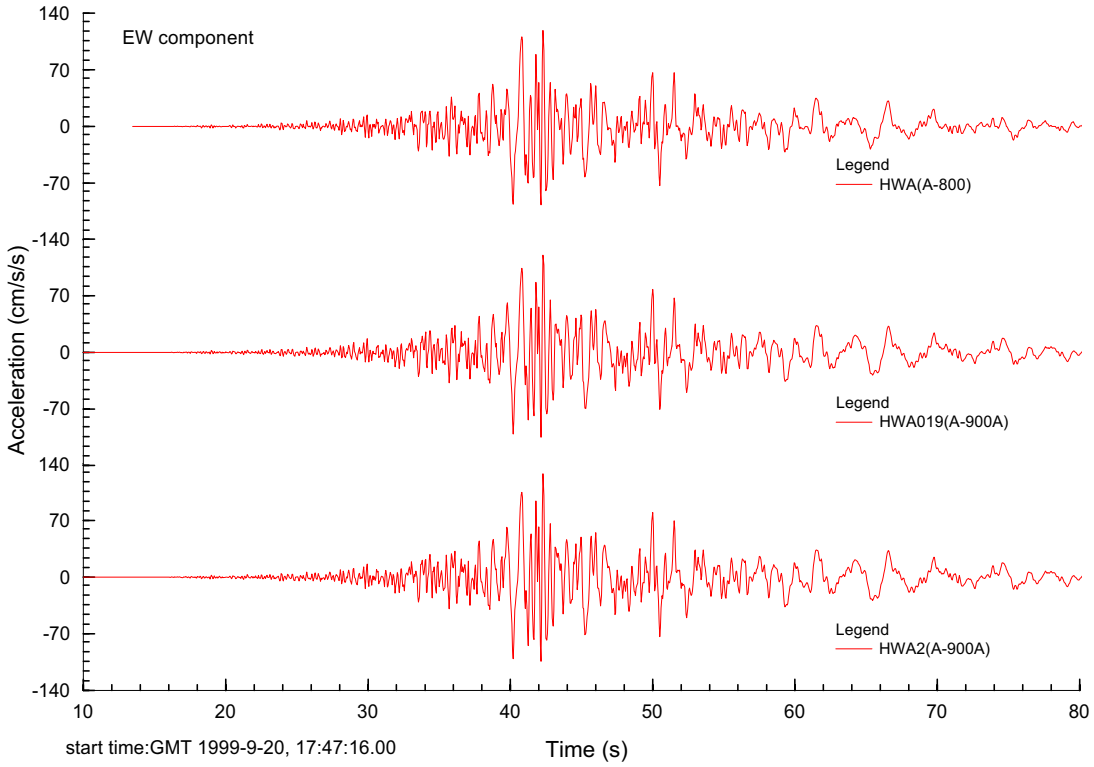

(c)

Figure 3. Comparisons of the three-component acceleration time series obtained from the three colocated instruments HWA(A-800), HWA019(A-900A) and HWA2(A-900A) for which the mean determined from a segment of the pre-event portion of the original record was removed from the whole record. The accelerograms are aligned according to the absolute GMT time of ground motion. The abscissa shows time relative to the GMT time Sep. 20, 1999, 17:47:16.00 (h:m:s).

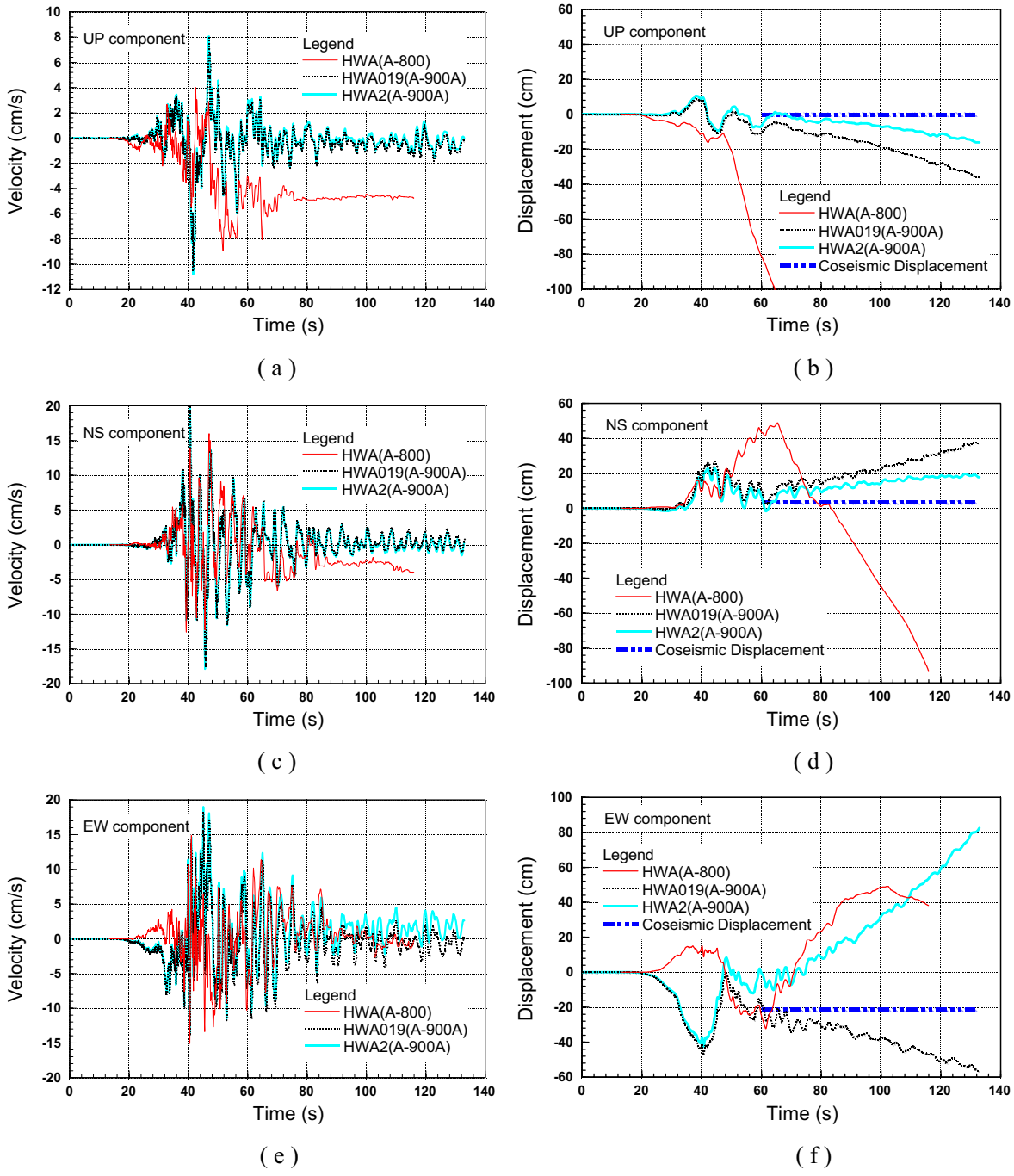

Figure 4. Comparison of uncorrected velocities and displacements obtained from the accelerations recorded by the three colocated instruments HWA(A-800), HWA019(A-900A) and HWA2(A-900A). The uncorrected velocities and displacements were obtained by single and double integration of accelerations for which the pre-event mean was removed from the whole trace. The GPS estimates of coseismic displacements are $-0.8 \pm 0.9cm$, 3.7 cm and -21.3 cm for the UP, NS and EW components, respectively, as obtained from a GPS instrument colocated with the accelerometers (Yu et al., 2001). The abscissa shows time relative to the GMT time Sep. 20, 1999, 17:47:16.00 (h:m:s).

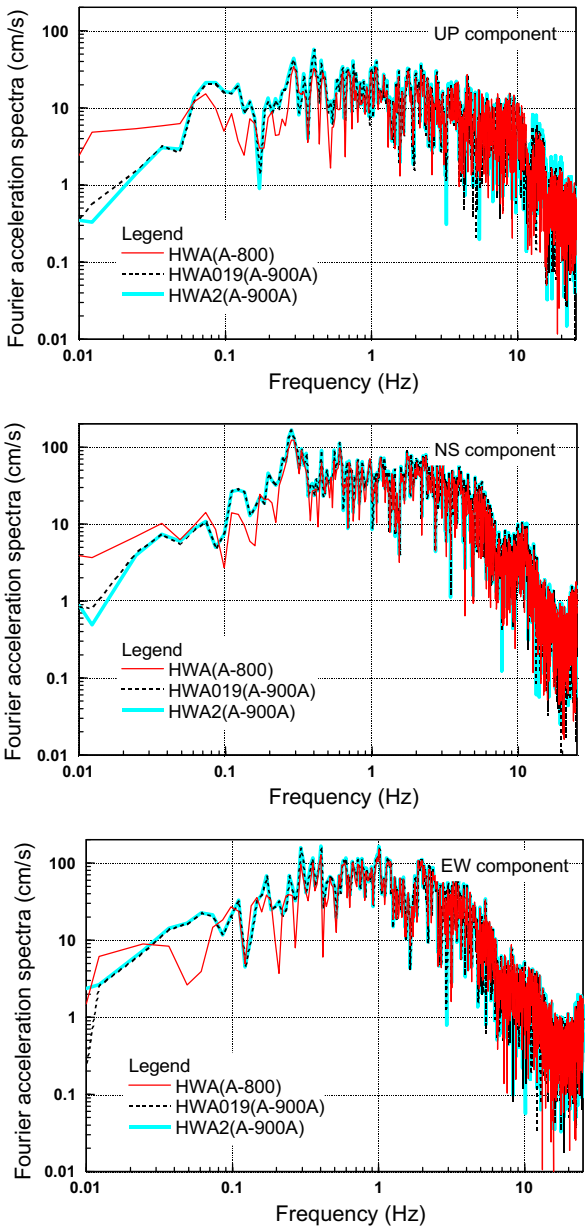

Figure 5. Fourier acceleration frequency spectra calculated from the uncorrected accelerations recorded by the three colocated instruments HWA(A-800), HWA019(A-900A) and HWA2(A-900A).

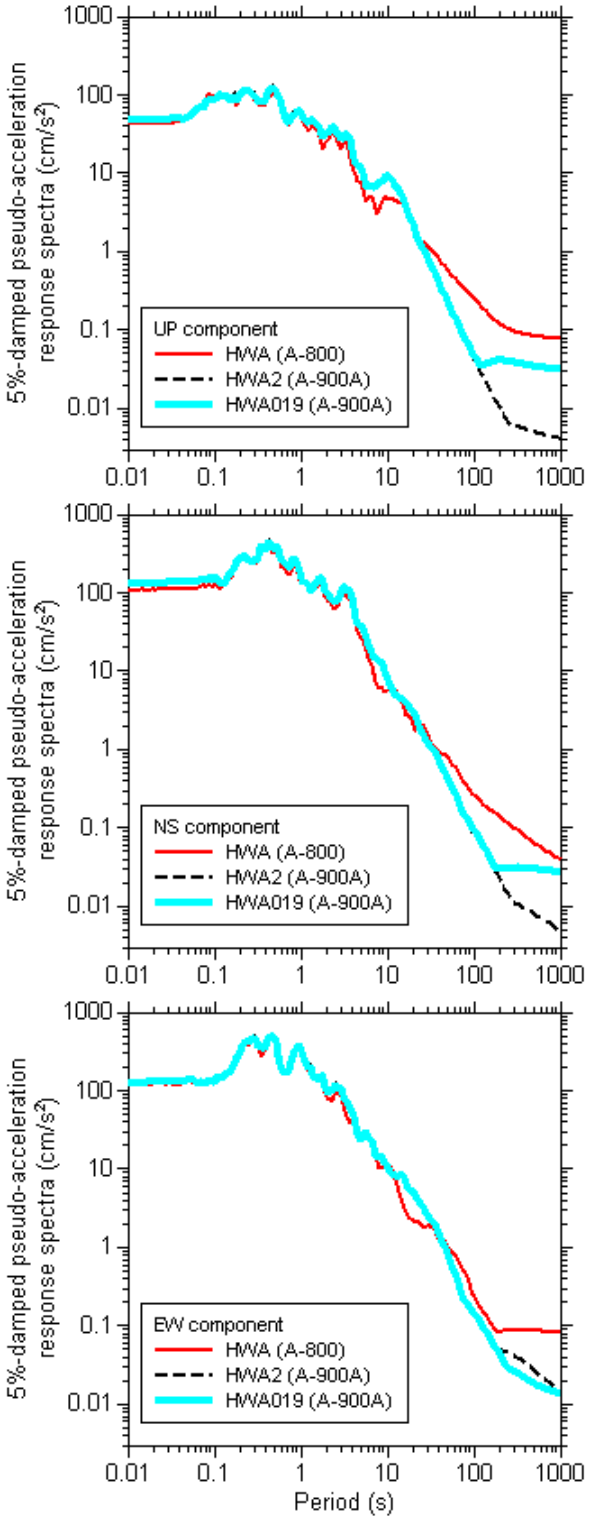

Figure 6. 5% damped pseudo-acceleration response spectra calculated from the uncorrected accelerations recorded by the three colocated instruments HWA(A-800), HWA019(A-900A) and HWA2(A-900A). Before computing the response spectra, zeros were added to the end of the acceleration time series so that the total duration exceeded the oscillator period.

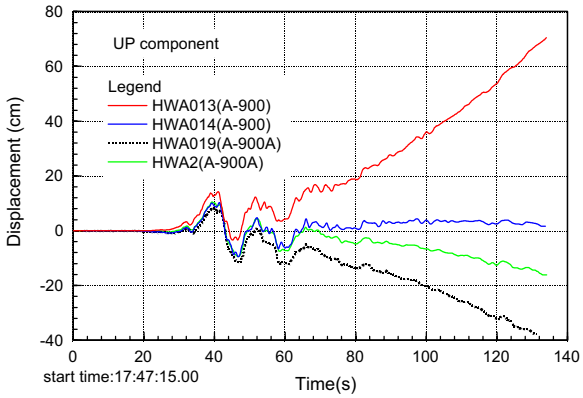

(a)

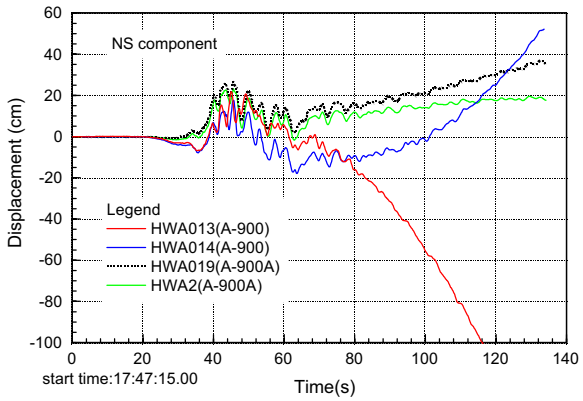

(b)

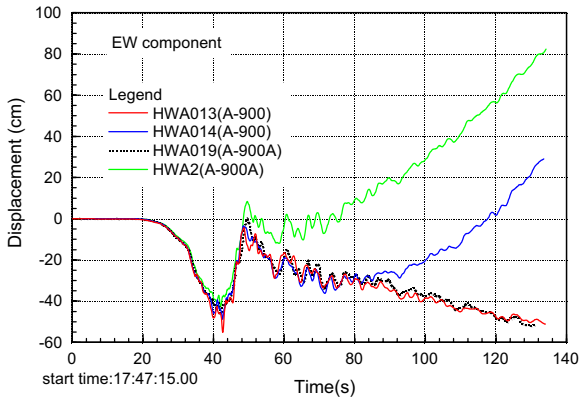

(c)

Figure 7. Comparison of uncorrected displacements obtained from four closely-spaced instruments HWA013(A-900), HWA014(A-900), HWA019(A-900A) and HWA2(A-900A) (HWA2 and HWA019 are colocated). The displacements are obtained from doubly-integrated uncorrected accelerations for which the mean of the pre-event portion has been removed from the whole acceleration trace. The abscissa shows time relative to the GMT time Sep. 20, 1999, 17:47:15.00 (h:m:s).

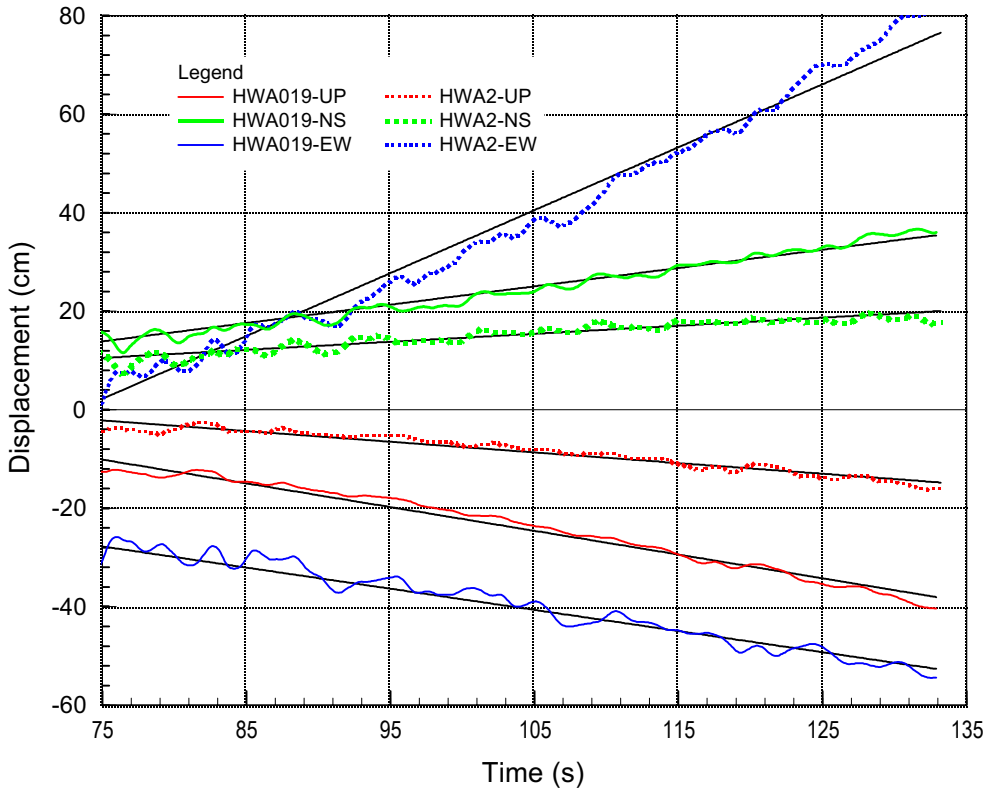

Figure 8. A small portion (70-130 sec) of the displacement time series of HWA019-UP, HWA2-UP, HWA019-NS, HWA2-NS, HWA019-EW, and HWA013-EW. The lines are the least-squeard fitted resulted from 70sec to the end. HWA013-EW

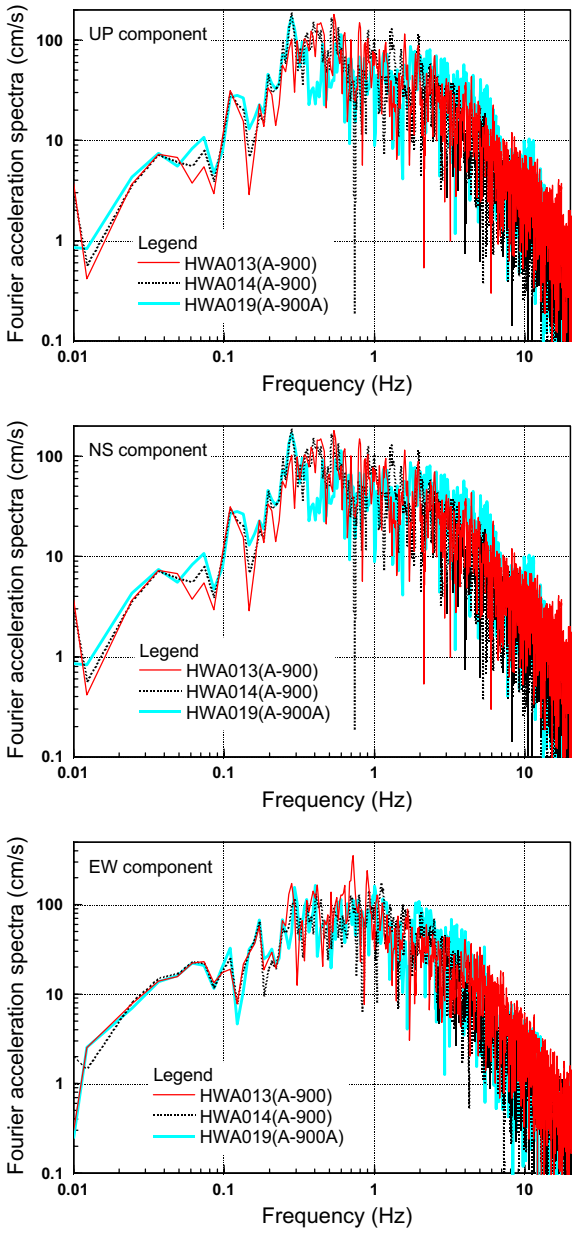

Figure 9. Fourier acceleration spectra calculated from the uncorrected accelerations recorded by the three closely-spaced (but not colocated) instruments HWA013(A-900), HWA014(A-900) and HWA019(A-900A). The Fourier frequency spectra of HWA2 are consistent with those of HWA019 in the whole frequency range as shown in the Figure 5, so the Fourier spectra of HWA2 are not shown in this figure.

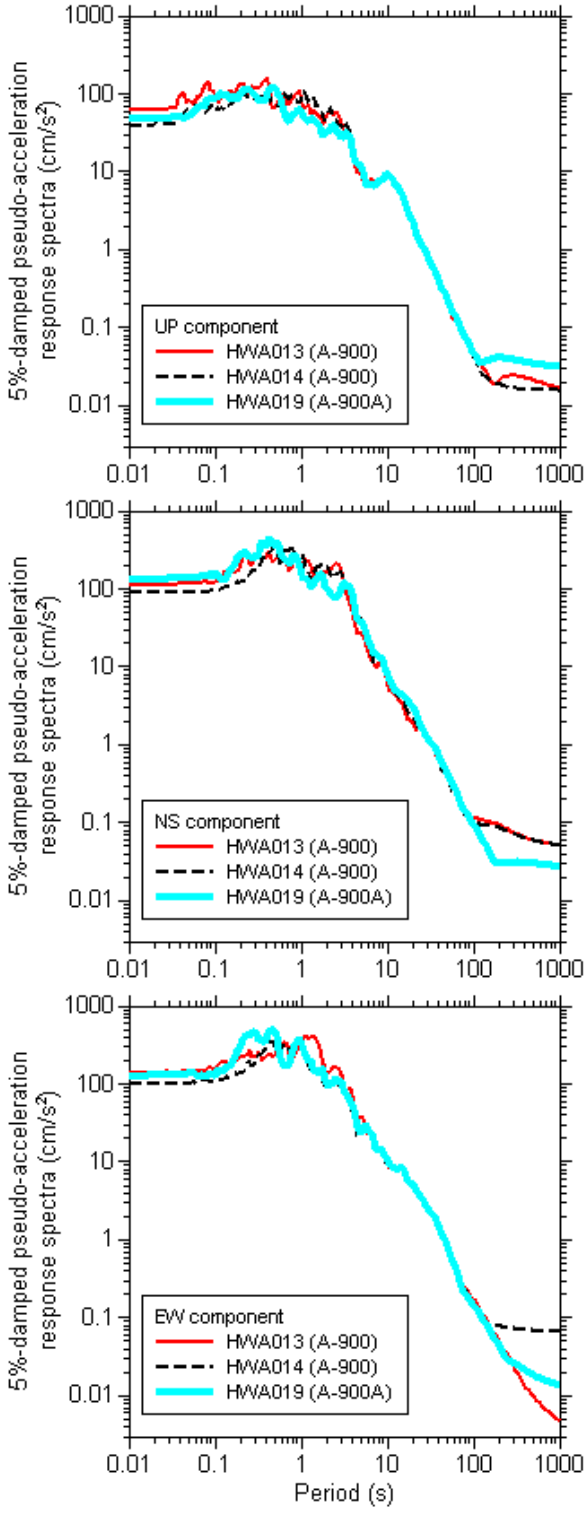

Figure 10. 5% damped acceleration response spectra calculated from the uncorrected accelerations recorded by the three closely-spaced (but not colocated) instruments HWA013(A-900), HWA014(A-900) and HWA019(A-900A). The response spectra of HWA2 are almost equal to those of HWA019 for periods less than 100 sec and are not shown here (see Figure 6 for a comparison over the whole period range). Before computing the response spectra, zeros were added to the end of the acceleration time series so that the total duration exceeded the oscillator period.

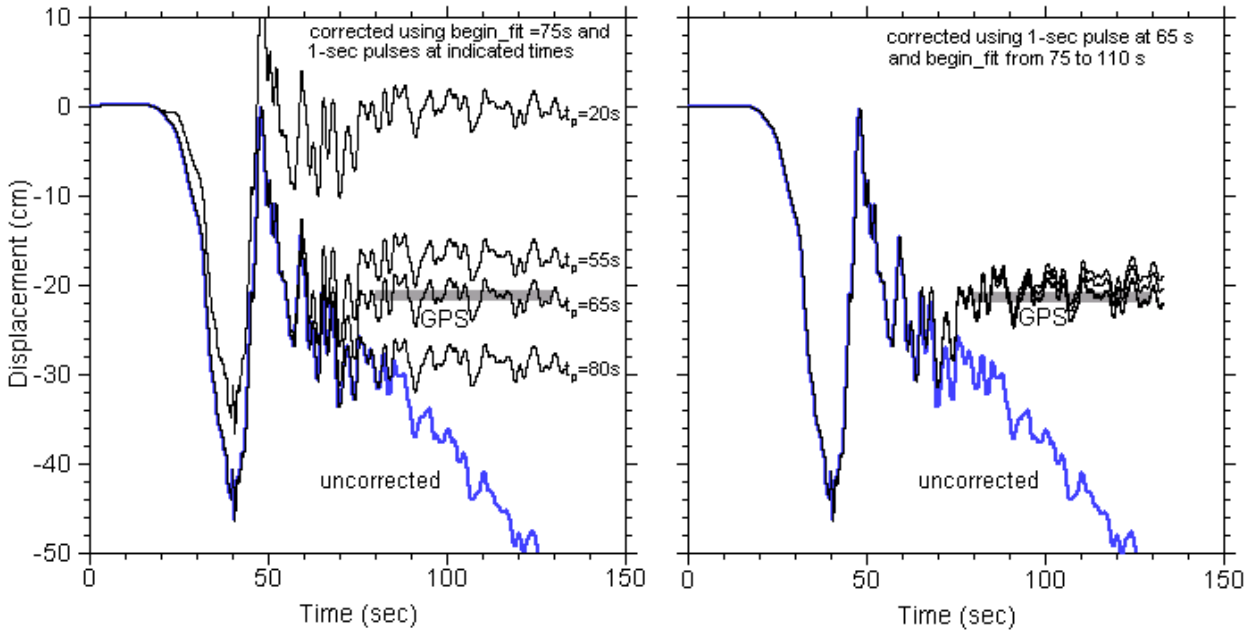

Figure 11. Displacement for HWA019-EW, corrected by assuming a 1 sec pulse in the acceleration baseline (the area under the pulse equals the step in velocity corresponding to the slope of a line fit to displacement). (left column) Placing the pulse at various times; (right column) Using various values of the beginning time used in the least-squares fitting of the straight line to the end of the displacement (the line was fit to the displacement from the time shown to the end of the record).

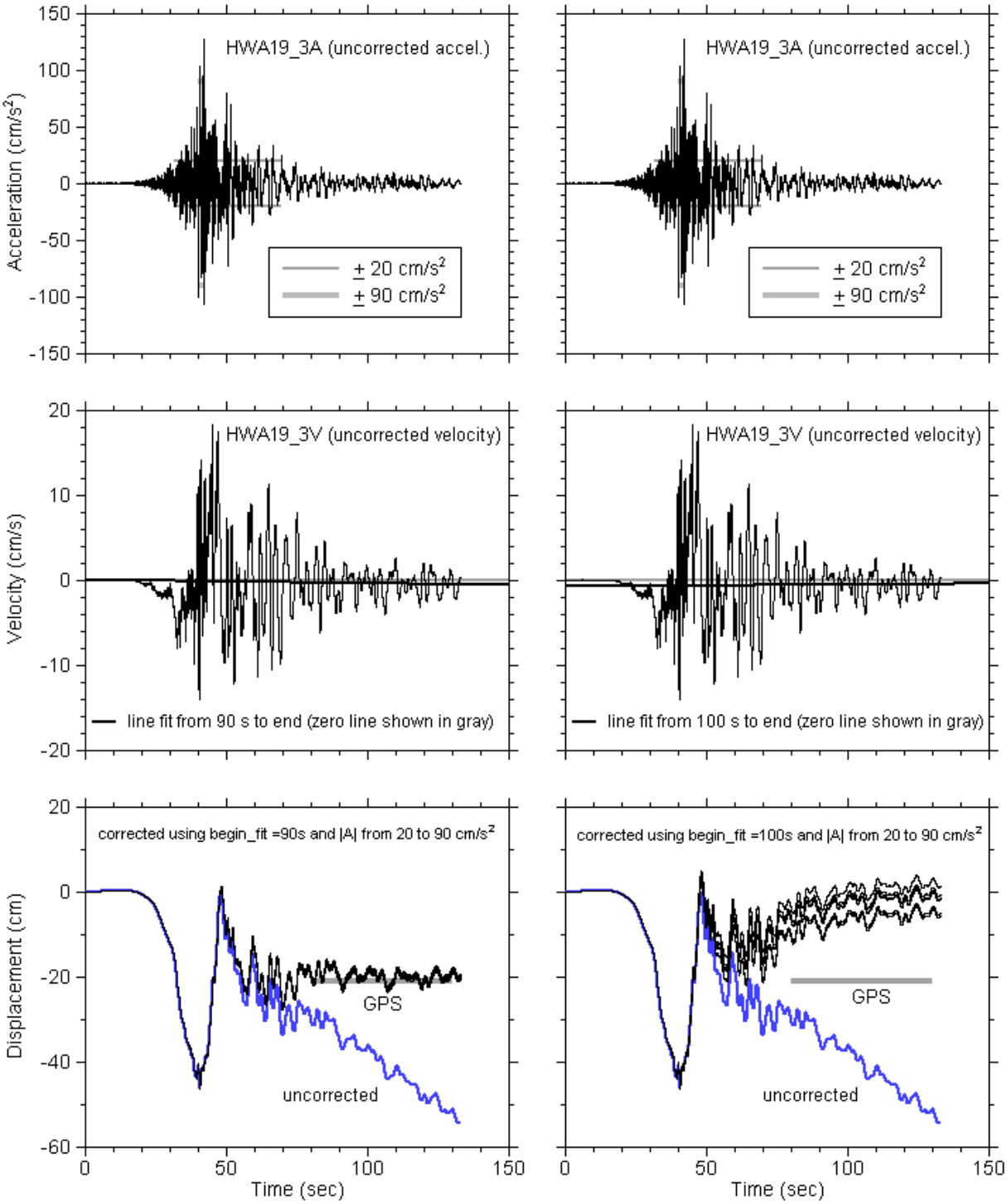

Figure 12. Displacement for HWA019-EW, assuming an Iwan et al. correction scheme (a pulse followed by a step in the acceleration baseline). Using different exceedance levels from 20 to 90 cm/s^2, (left column) the beginning time used in the least-squares fitting of the straight line is 90 sec(t2b=90 sec); (right column) the beginning time used in the least-squares fitting of the straight line is 100 sec (t2b=100 sec).

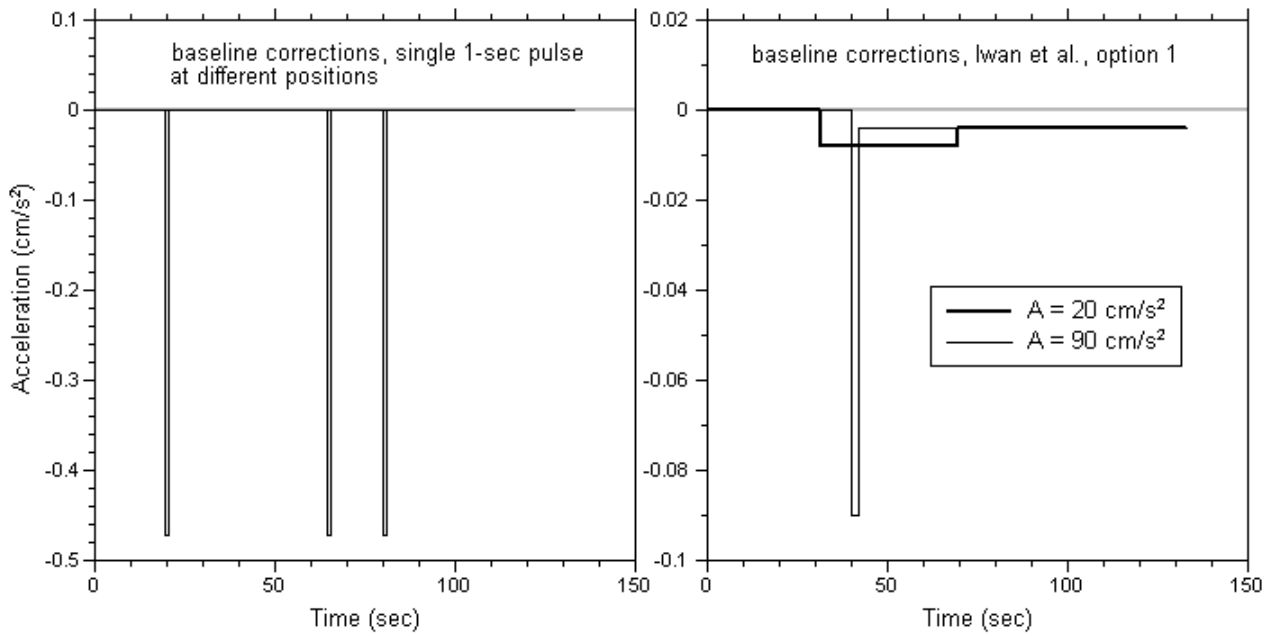

Figure 13. The baseline corrections (removed baseline offsets) for several of the corrections used to produce the displacements in Figures 11 and 12.

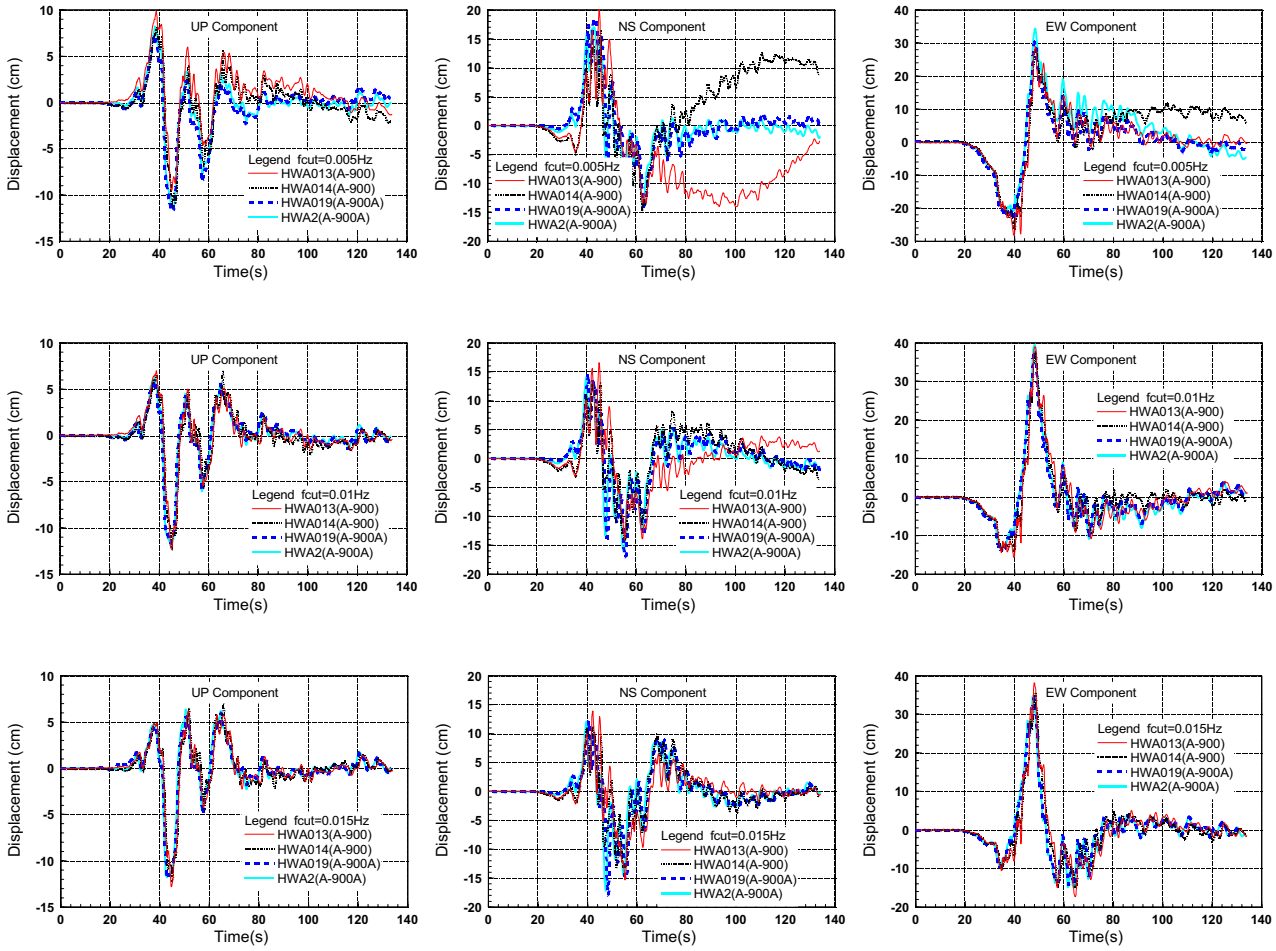

Figure 14. The filtered three-component displacements obtained by integration of the accelerations recorded by the closely-spaced instruments HWA013, HWA014, HWA019 and HWA2 (the latter two are colocated). The start time of the time axes is GMT 17:47:15.00. A fourth-order Butterworth causal low-cut filter was applied to the uncorrected accelerations. (upper row): 0.005 Hz low-cut filter; (middle row): 0.01 Hz low-cut filter; (lower row): 0.015 Hz low-cut filter.

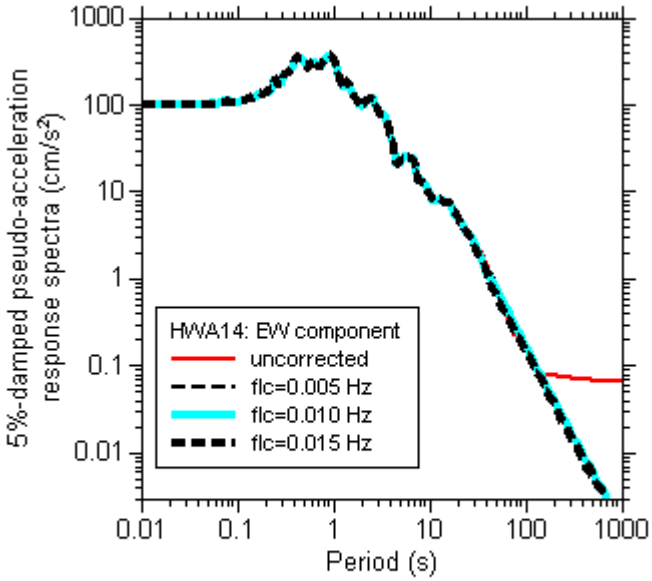

Figure 15. 5% damped pseduo-acceleration response spectra calculated from the uncorrected and a series low-cut filtered (fcut=0.001Hz, 0.003Hz, 0.01Hz, 0.03Hz, and 0.1Hz) accelerations recorded by the EW component of HWA014 (A-900).